Prompt fission neutron (PFN) emission in $^{235}U(n_{th}, f)$ reaction

Zeynalov Sh. Sedyshev P., Sidorova O., Shvetsov V.

JINR-Joint Institute for Nuclear Research, Dubna, Russia

ISINN-26, May-June 2018, Xi'an, China

1. Motivation

The mechanism of PFN emission in fission plays important role in nuclear fission theory from the one hand and the information on PFN is highly demanded by nuclear power industry from the other hand.

Analysis of TKE measured in resonance neutron induced fission of ^{235}U revealed surprising fluctuation. The recent measurement of PFN multiplicity in ^{235}U resonances demonstrates fluctuations of PFN multiplicities to.

One of the interesting observation is the increasing $\bar{\nu}(A)$ from the heavy FF only with increase of the excitation energy of fissioning system still has no clear explanation

In current report we presenting some preliminary results of measurement of PFN emission in thermal neutron induced fission of ^{235}U reaction as test of apparatus for resonance neutron induced fission of ^{235}U measurements foreseen to perform at IREN facility next year

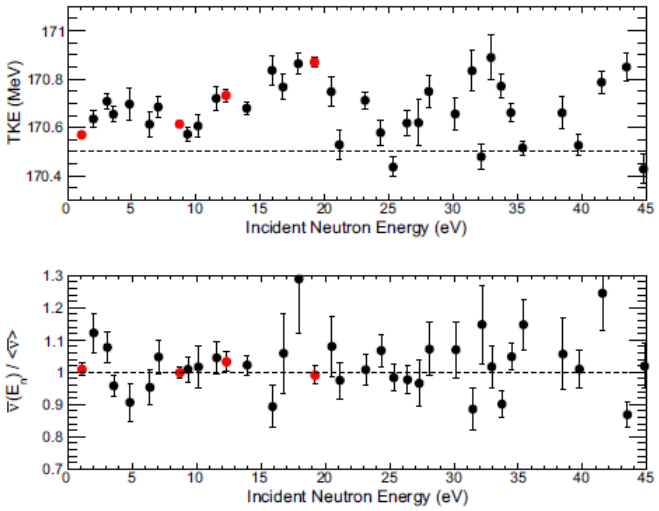

EPJ Web of Conferences **111**, 05001 (2016)
DOI: 10.1051/epjconf/201611105001

2. Experimental setup and data acquisition system.

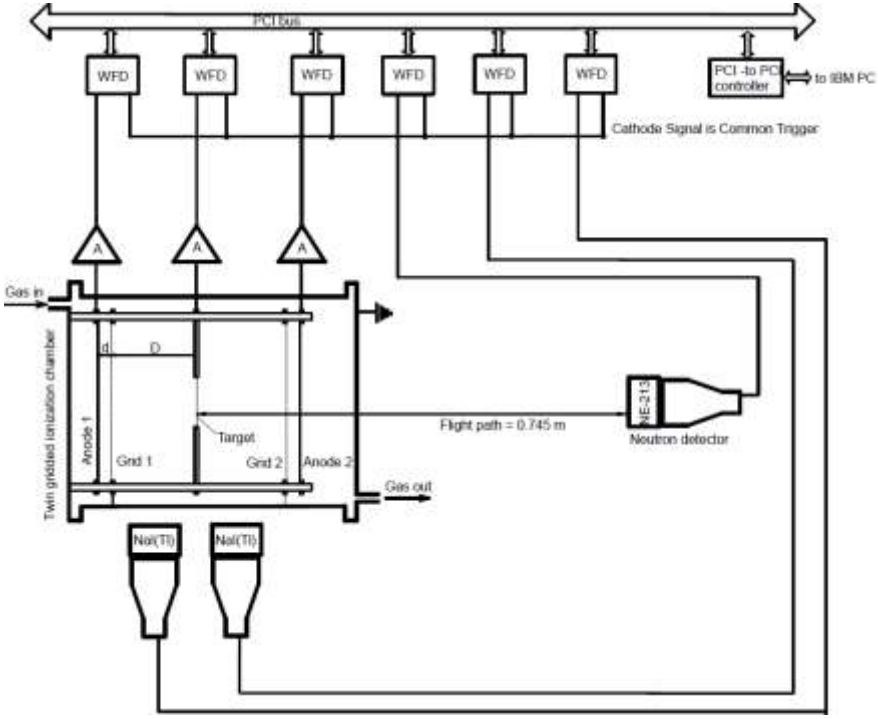

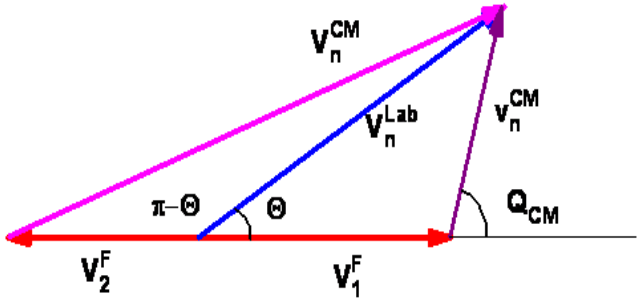

$$\bar{\nu}(A)=\frac{\int_0^\infty \nu(A,TKE)Y(A,TKE)dTKE}{\int_0^\infty Y(A,TKE)dTKE},\quad \bar{\nu}=\int_0^\infty \nu(A,TKE)Y(A,TKE)dTKEdA,\quad 200=\int_0^\infty Y(A,TKE)dTKEdA$$

$$\bar{\nu}(TKE)=\frac{\int_0^\infty \nu(A,TKE)Y(A,TKE)dA}{\int_0^\infty Y(A,TKE)dA},\quad \bar{\nu}=\int_0^\infty \nu(A,TKE)Y(A,TKE)dTKEdA,\quad 200=\int_0^\infty Y(A,TKE)dTKEdA$$

Adopted from C. Budtz-Jørgensen and H.-H. Knitter, *Nucl. Phys.*, A490, 307(1988) and modified with digital pulse processing apparatus

3. Digital Pulse Processing (DPP).

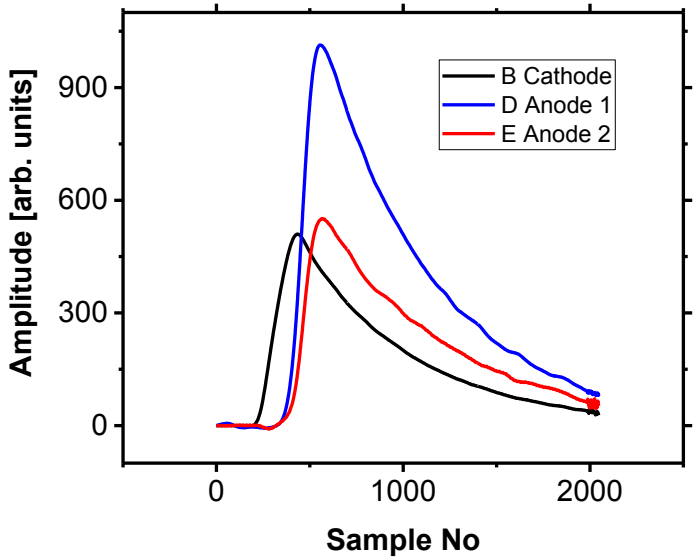

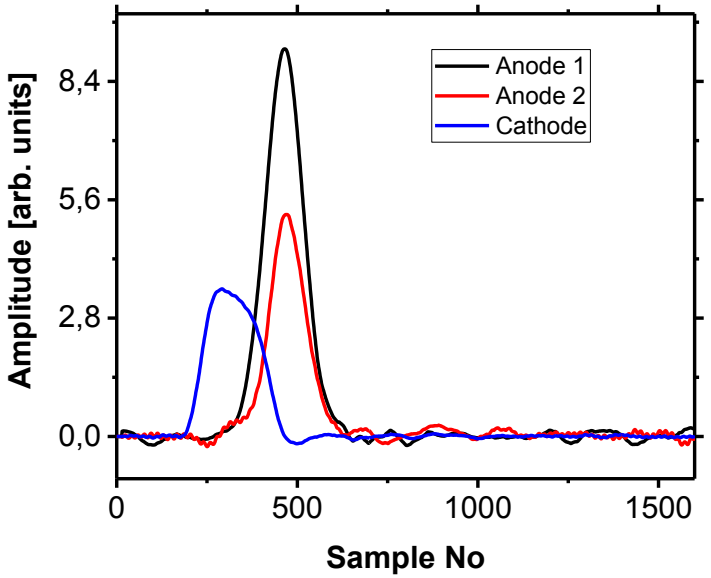

In our approach we have oversampled FF signals. The oversampling we used to increase the effective number of bits (ENOB) improving the signal representation. In practice the increase of ENOB realized automatically when signal passed through second order low pass filter :

$$V^1_{out}(t) = \int_0^{\infty} V_{in}(\xi) \bullet \exp(-\frac{(\xi - t)}{\tau}) d\xi,\ V^2_{out} = \int_0^{\infty} V^1_{out}(\xi) \bullet \exp(-\frac{(\xi - t)}{\tau}) d\xi$$

Improved signal presentation (left figure) facilitates numerical solution (differentiation) of the integral equation

$$V(t) = Const \bullet \int_0^t i(\xi) \exp(-\xi / \tau) d\xi$$

Solution of the equation is i(t) presented on the right figure for the cathode and two anode signals. In terms of familiar analog electronics the operation performed equivalent to differential filter on the input of spectroscopy amplifier (SA). To simulate integrating stage of the SA we implemented integration according to

$$V(t) = \int_0^t i(\xi) d\xi$$

The last operation, performed with two correlated anode waveforms, provides the pulse heights of FF.

4. Drift time determination of FF ionization

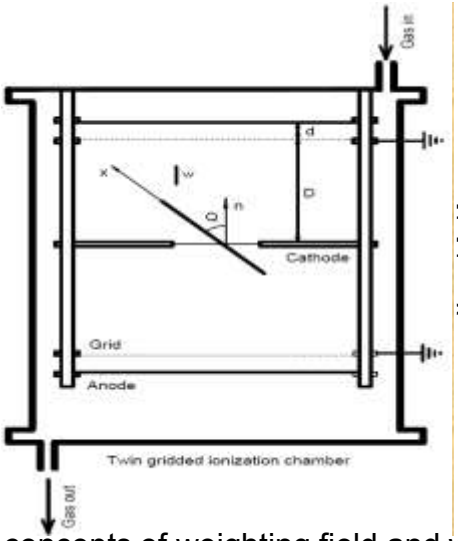

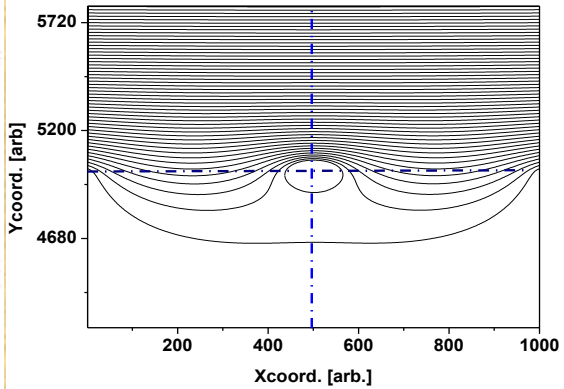

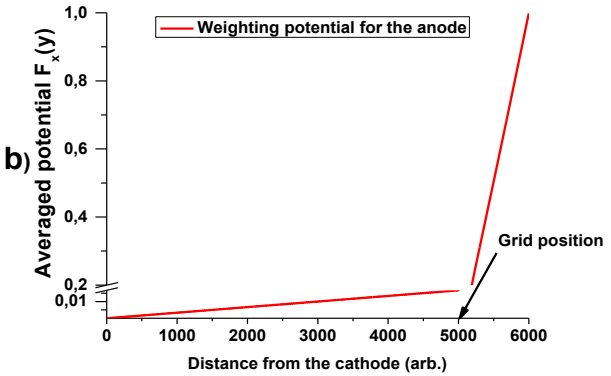

The concepts of weighting field and weighting potential states that the instantaneous current induced on a given electrode is equal to $i = q\bar{v}E_0$, where *q* is the charge of the carrier, $\bar{v}$ its velocity, and E_0 is called the weighting field. Another way of stating the same principle is that the induced charge on the electrode is given by the product of the charge of the carrier multiplied by the difference in the weighting potential from the beginning to the end of the carrier path $Q = q\Delta\Phi$. The weighting potential as a function of position was found as the solution of the Laplace equation for the geometry of the detector with special boundary conditions. Evaluation of the drift time can be done if the weighting potential inside the sensitive volume of the chamber is calculated as shown in the above graphs. Using explicit functions for weighting potential one can find the following expression for drift time T for ionization charge density shifting from the origin to the anode:

$$T = \frac{D}{W} \bullet \left\{ (1 - \frac{\overline{X}}{D} \bullet \cos(\Theta)) + \frac{d}{2 \bullet D} \bullet (1 - \frac{\sigma}{1-\sigma} \bullet (1 - \frac{\overline{X}}{D} \cos(\Theta)) \right\},$$

where the meanings of d, D, Θ are clear from the sketch of the TBIC, ϭ is the grid inefficiency factor or it is the value of the average weighting potential at grid location, and X is the center for ionization charge distribution along the FF track. Parameter T for corresponding anode can be measured using the signal current waveform as follows

$$T = S / S_0, \text{ where } S = \int_0^{T_{\max}} i(t) * t dt, \; S_0 = \int_0^{T_{\max}} i(t) dt$$

5. FFs pulse height correction and cos(Θ) evaluation

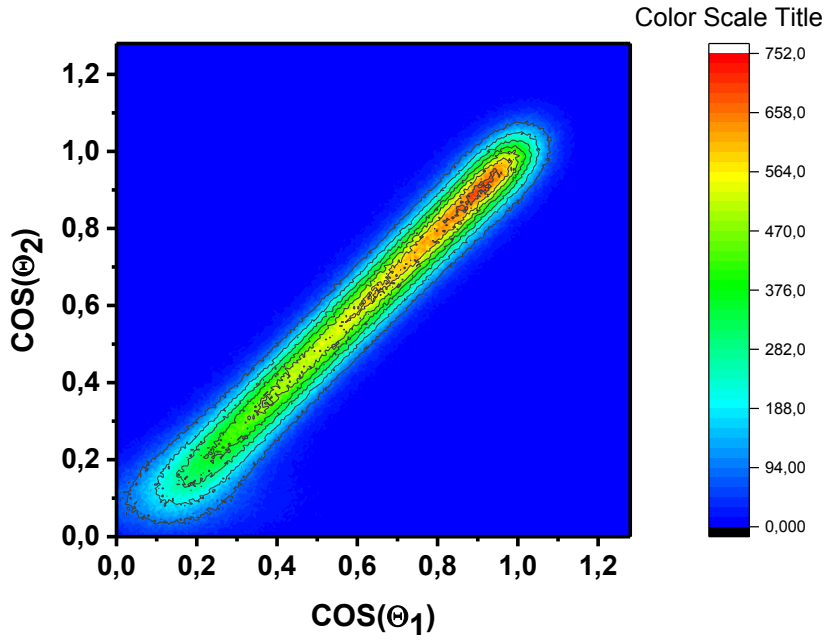

$$T = \frac{D}{W}\cdot\left\{(1-\frac{\overline{X}}{D}\cdot\cos(\Theta))+\frac{d}{2\cdot D}\cdot(1-\frac{\sigma}{1-\sigma}\cdot(1-\frac{\overline{X}}{D}\cdot\cos(\Theta))\right\}$$

$$T_0 = T(\cos(\Theta)=1)$$

$$\mathrm{T}_{90} = T(\cos(\Theta)=0)$$

$$\cos(\Theta) = \frac{T_{90}-T}{T_{90}-T_0}$$

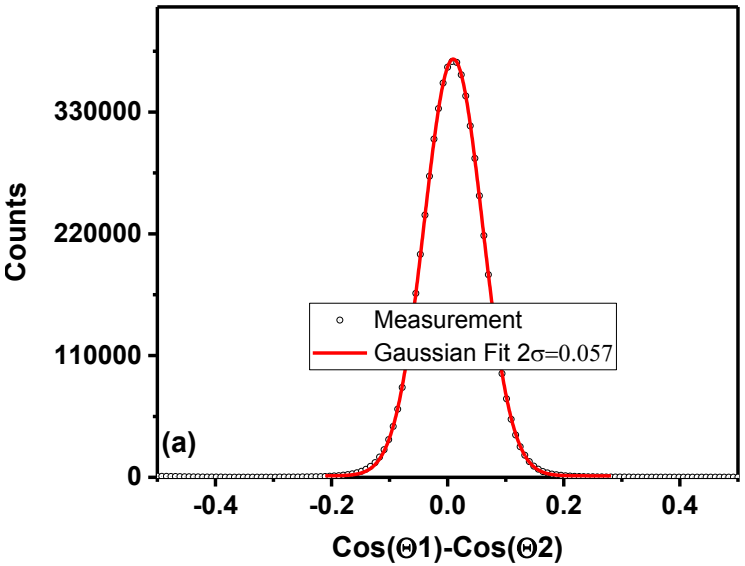

Cosines calculated from measured drift times T according to formulae above are plotted as the difference of cosines measured for correlated FF in two halves of TGIC to demonstrate the quality of the algorithm.

$$P_A^C = P_A/(1-\sigma(1-\frac{T}{T_{90}})\bullet(1+\frac{d}{2D}))$$

6. FFs pulse height correction and using evaluated cos(Θ)

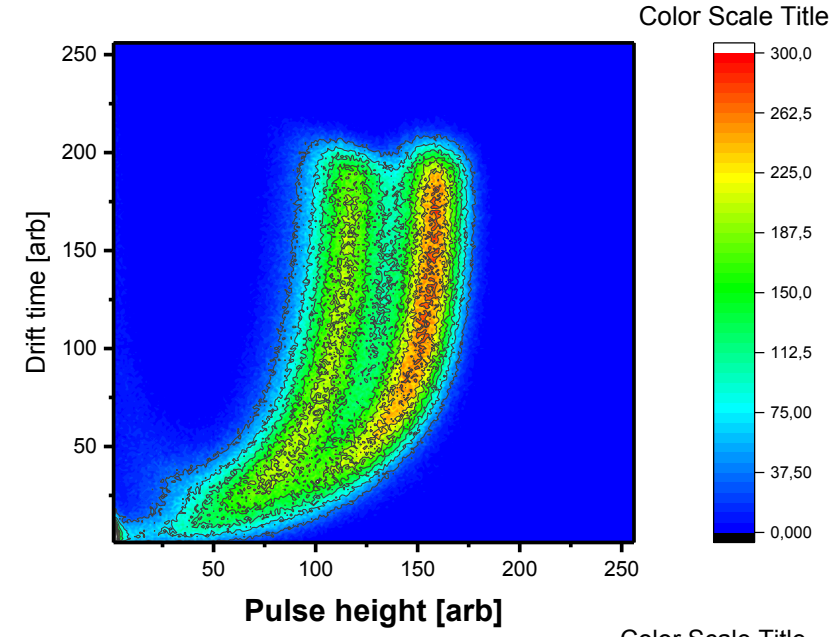

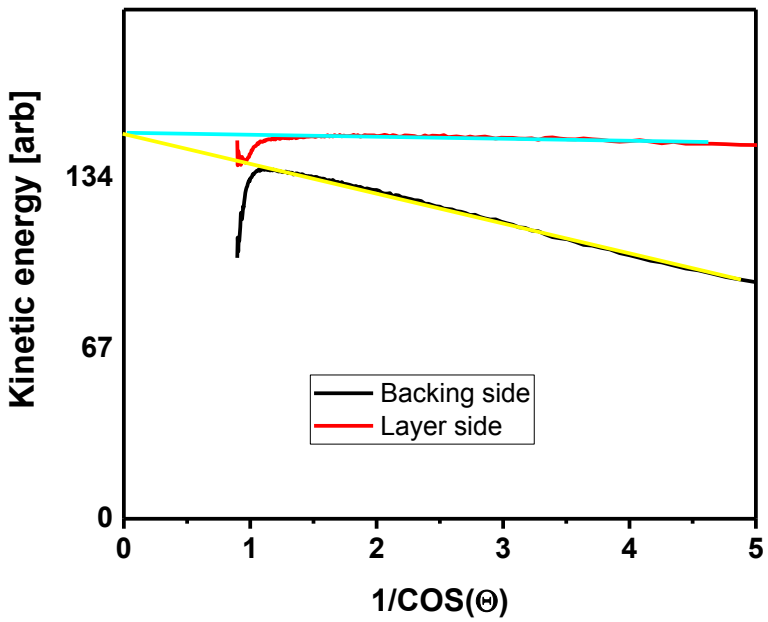

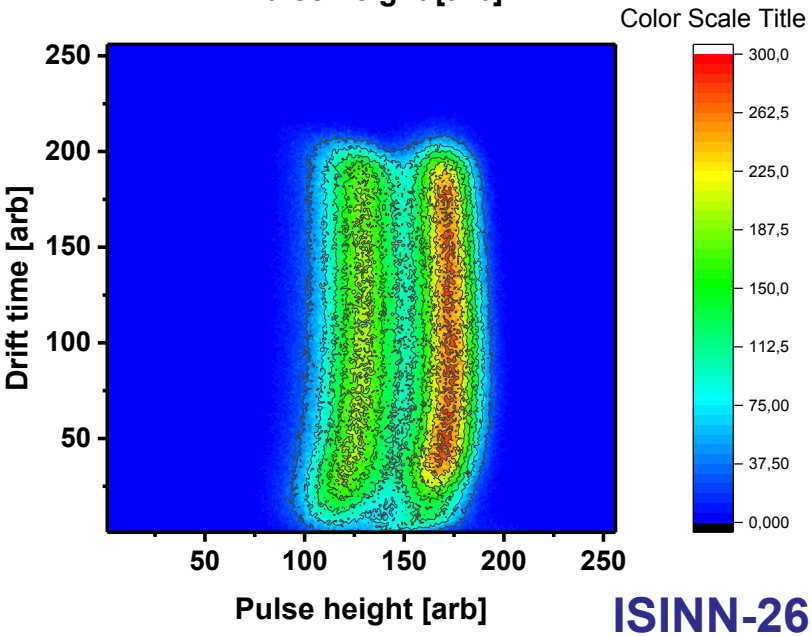

When FF pass the target it losses kinetic energy due to ionization. The longer the path more the energy loss. That's why the energy losses inversly proportional to the cosine between FF velocity and the normal to the target surface. Measurement the shift of double humped FF distribution for different invers cosine provide the measure of the energy losses for FF in the layer and backing sides of the target. This was the first correction of the FF kinetic energy for losses in the target.

7. PHD correction

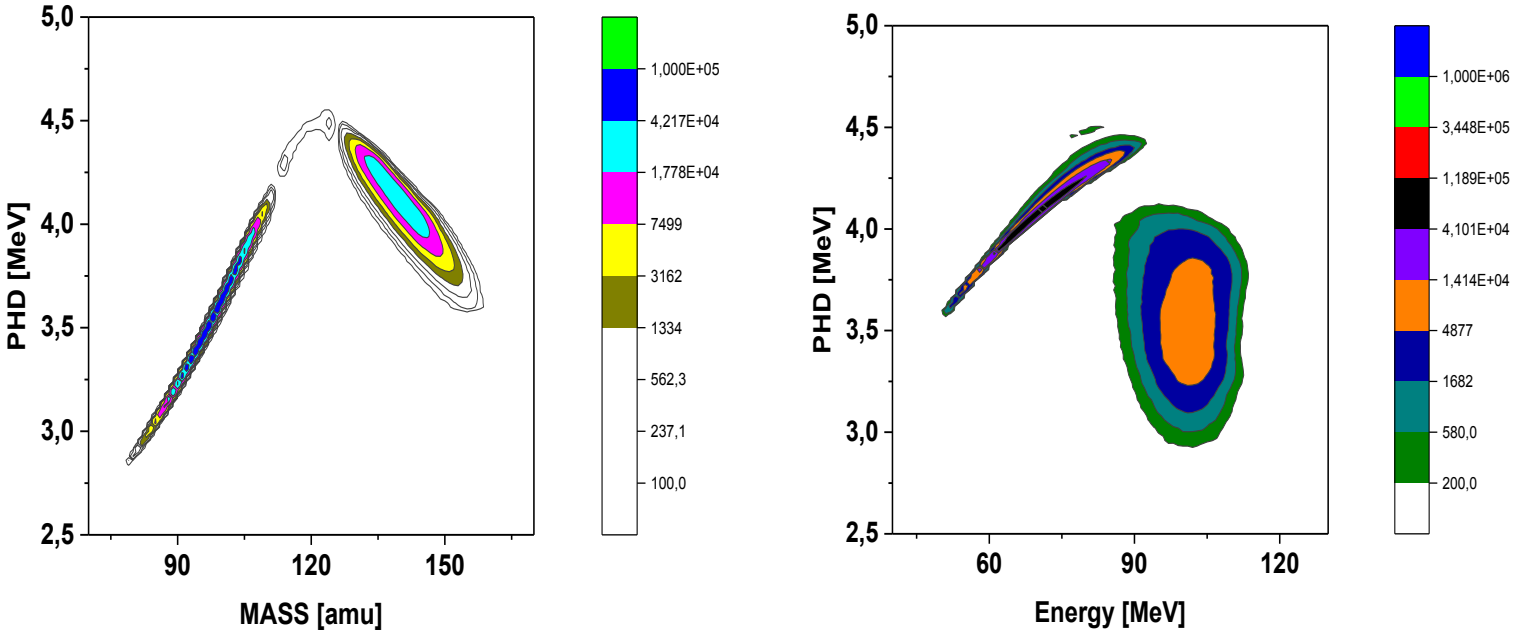

$$PHD(A_{post}, E_{post}) = \frac{A_{post} * E_{post}}{\alpha} + \frac{A_{post}}{\beta}$$

The correction for FF pulse height caused by momentum transfer to working gas atoms by FF (non ionizing collisions) during its deceleration – is called pulse height defect (PHD). The PHD depends on the FF mass and kinetic energy and was corrected in data analysis using parameterization suggested in **Ref.:** F.-J. Hambsch, J. van Aarle, and R. Vogt, Nucl. Instrum. and Meth. A361, 257 (1995) . Figures above plotted dependence of the value of the corrections on FF mass and kinetic energy values. In our experiment the correction both the values of parameters α and β was set to 1 because we used the P10 working gas.

8. FF mass energy distribution.

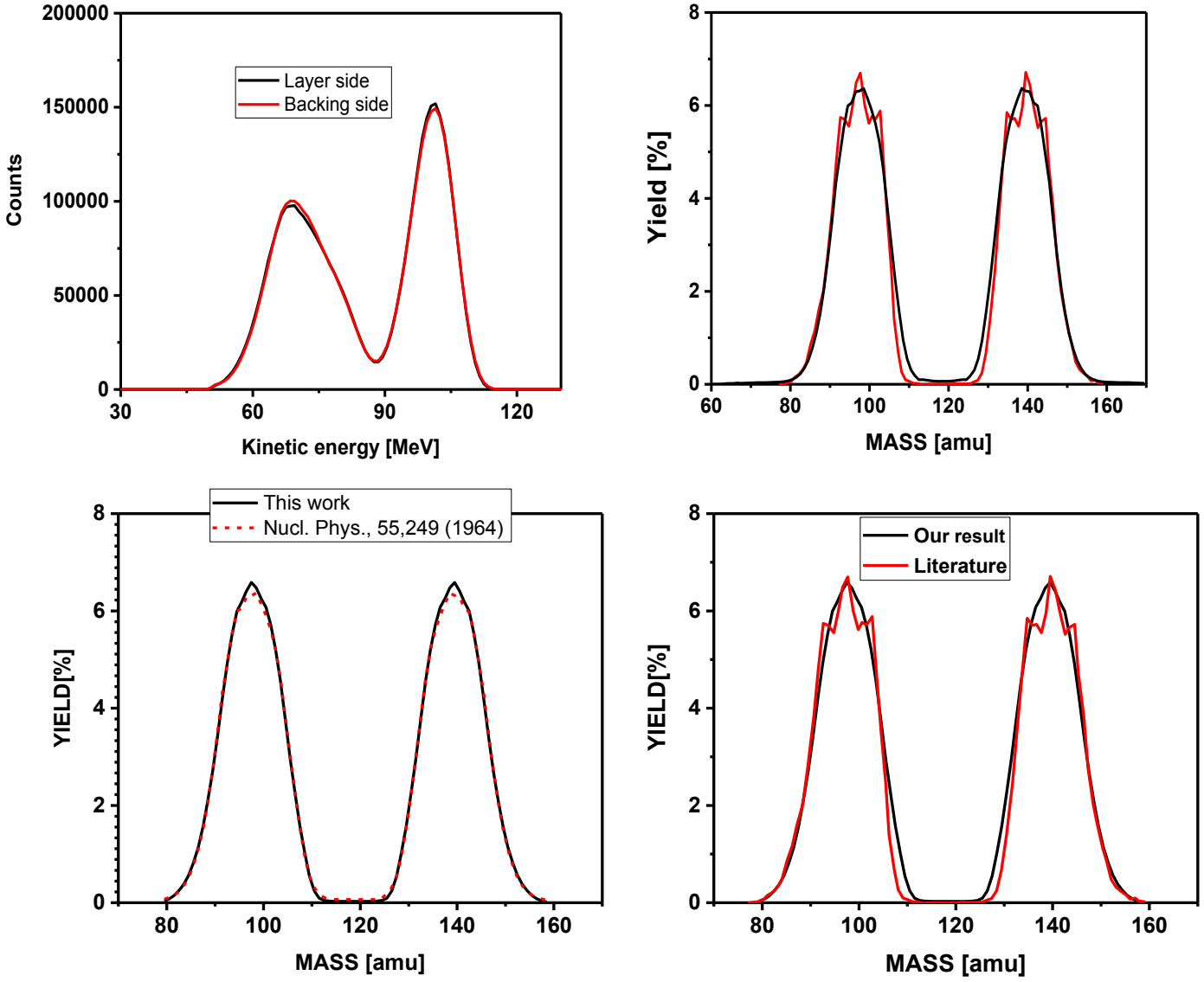

9. Constant fraction time marking for PFN TOF measurement

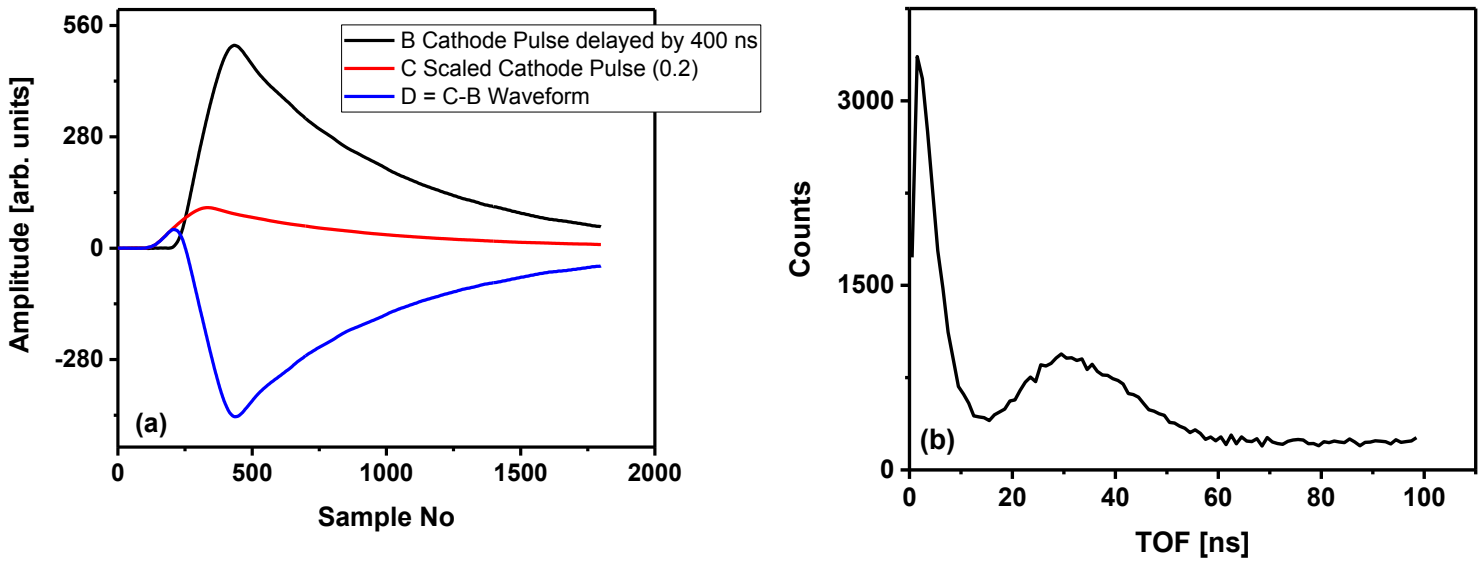

Constant fraction time marking (CFTM) method was implemented in the experiment for PFN time-of-flight evaluation. Figures demonstrate the method applied to the neutron detector signal. In conventional analog electronics the CFTM method the original signal first scaled by factor 0.2 and delayed for 0.1 of the pulse rise time. Then the delayed and scaled signal subtracted from the original one, producing bipolar pulse with zero crossing point assigned to time of the signal origin. This algorithm was applied to ionization chamber's cathode and the neutron detector signal. The difference between two signals was threated as TOF value and plotted on the right plot.

10. Neutron separation from gamma radiation

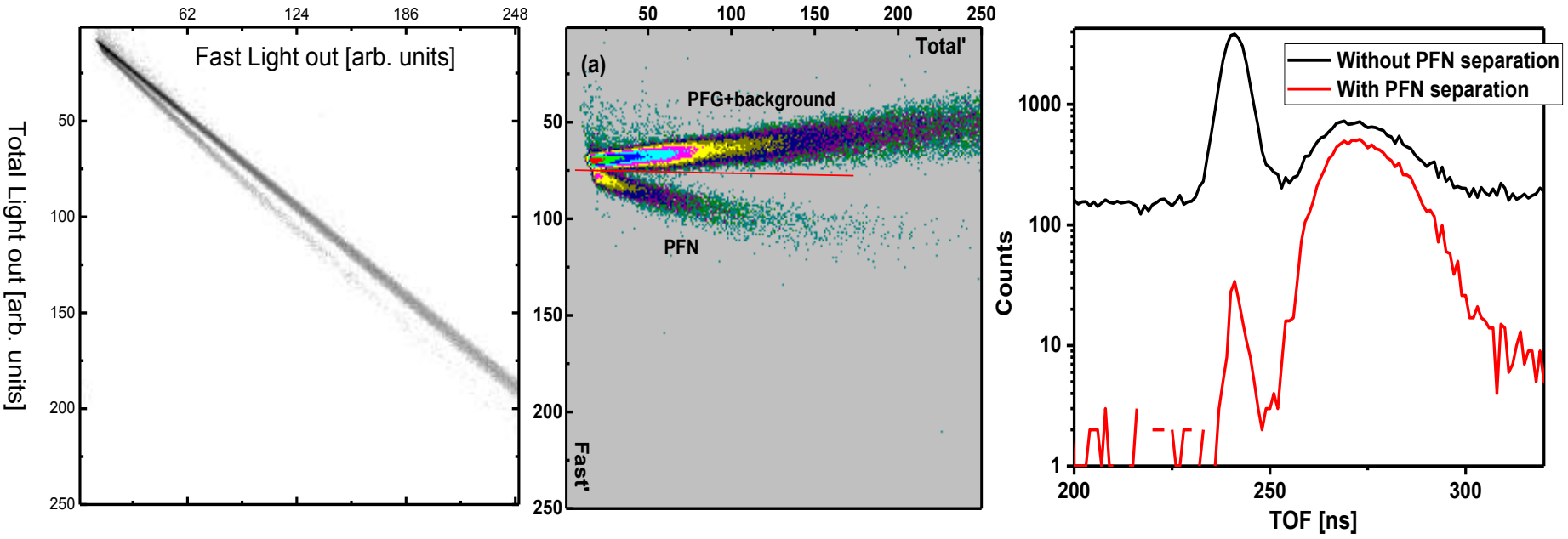

The two window algorithm (fast and total light output component) was implemented and resulted function *ND(Fast,Total)* was plotted on the left and middle figs. demonstrates the function *ND(Fast,Total)* in the reference frame rotated according to equation

$$F' = F \bullet \cos(\Omega) + T \bullet \sin(\Omega), T' = S \bullet \{-F \bullet \sin(\Omega) + T \bullet \cos(\Omega)\}$$

,where Ω – is axes rotation angle and S>1 – is the scaling factor. Red line in the middle figure is PFN-PFG separation line . Lower figure demonstrates the TOF distribution before and after PFN separation.

11. PFN angular distribution measurement

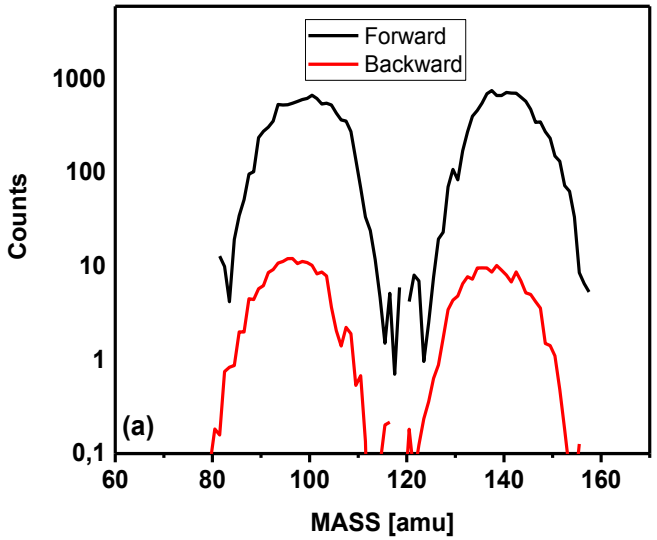

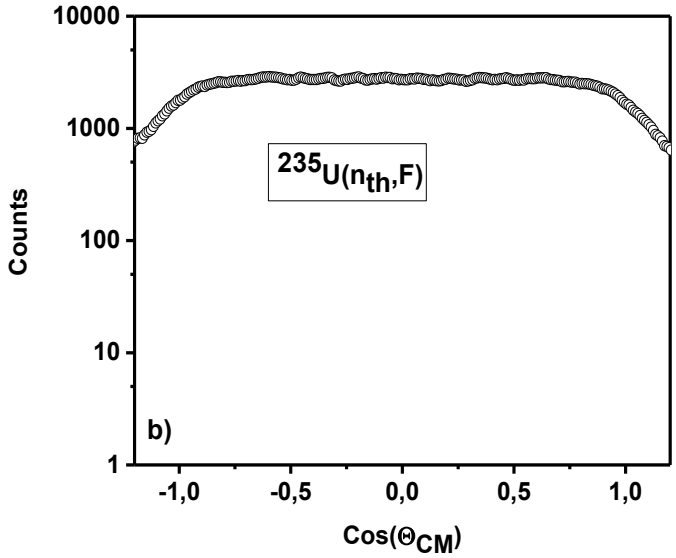

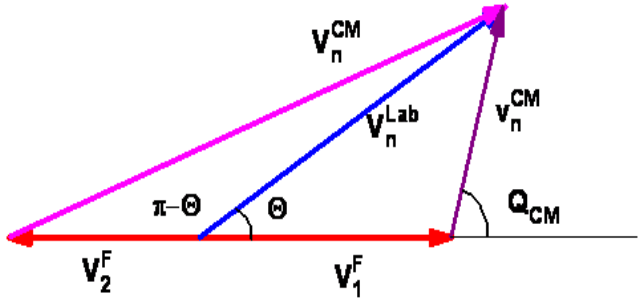

$$W_x = 1,\ W_y = \exp(E_{CM}^x - E_{CM}^y)$$

C. Budtz-Jorgensen and H.-H. Knitter, Nucl. Phys., A490, 307 (1988)

12. ND efficiency evaluation for 235U(n,f)

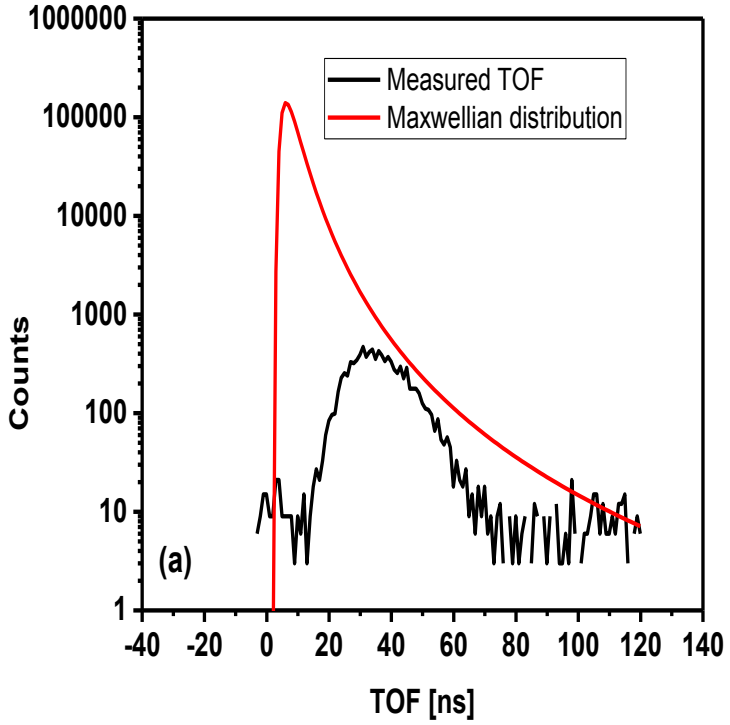

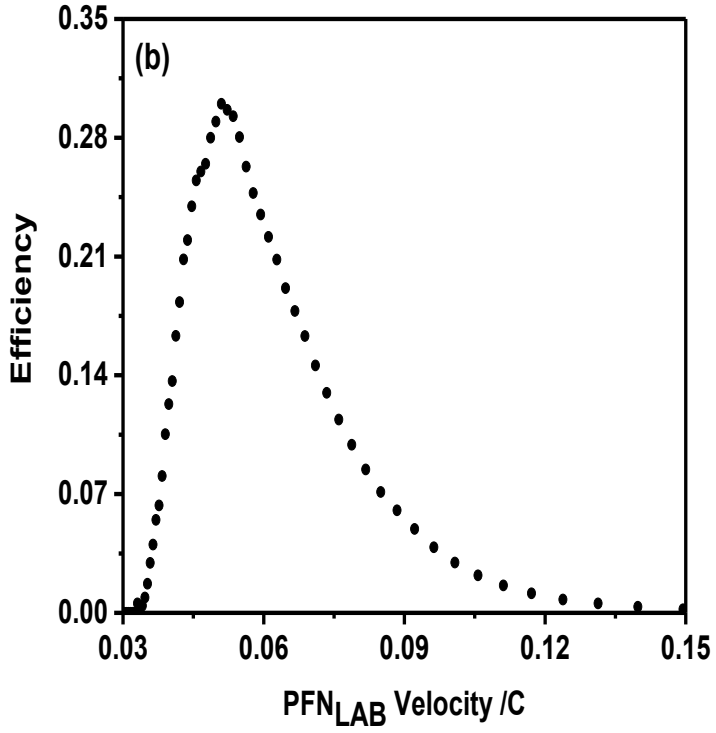

The neutron detector PFN detection efficiency was evaluated by comparison of the measured TOF distribution with the Maxwellian distribution with T=1.42 MeV.
Result is plotted on the right graph as detector efficiency dependence on PFN velocity and was used for average PFN number correction for evaluation of PFN dependence on FF mass and TKE.

13. PFN multiplicity on FF mass evaluation from measured data

$$\bar{\nu}(A) = \int_0^{\infty} \frac{Yc(A, TKE, V_{LAB}) \bullet V_{CM} \bullet (V_{LAB} - V_F \bullet \cos(\Theta))}{\varepsilon(V_{LAB}) \bullet V_{LAB}^2} dV_{LAB} dTKE \Big/ \int_0^{\infty} Y(A, TKE) dTKE$$

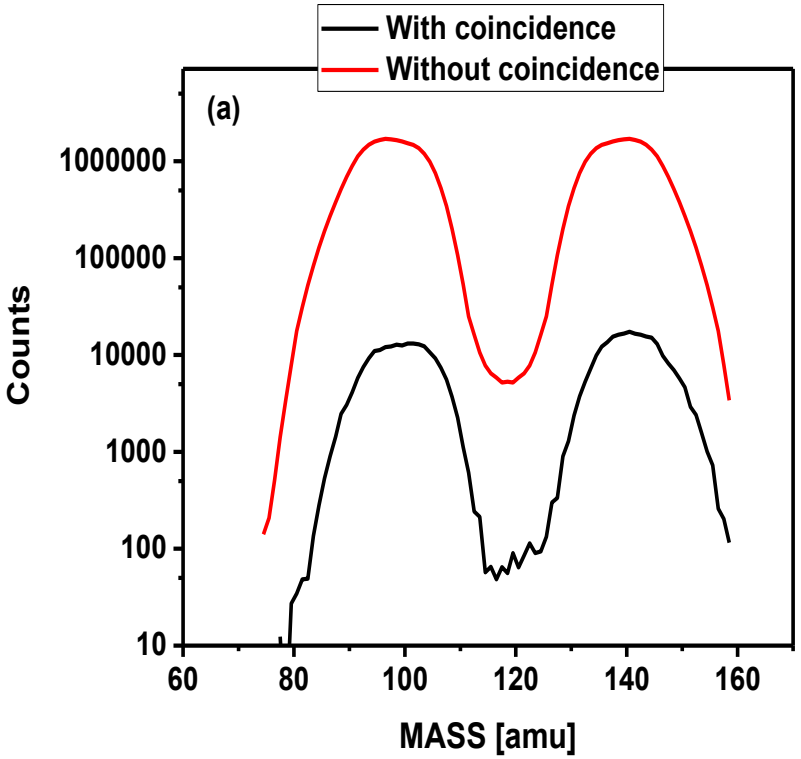

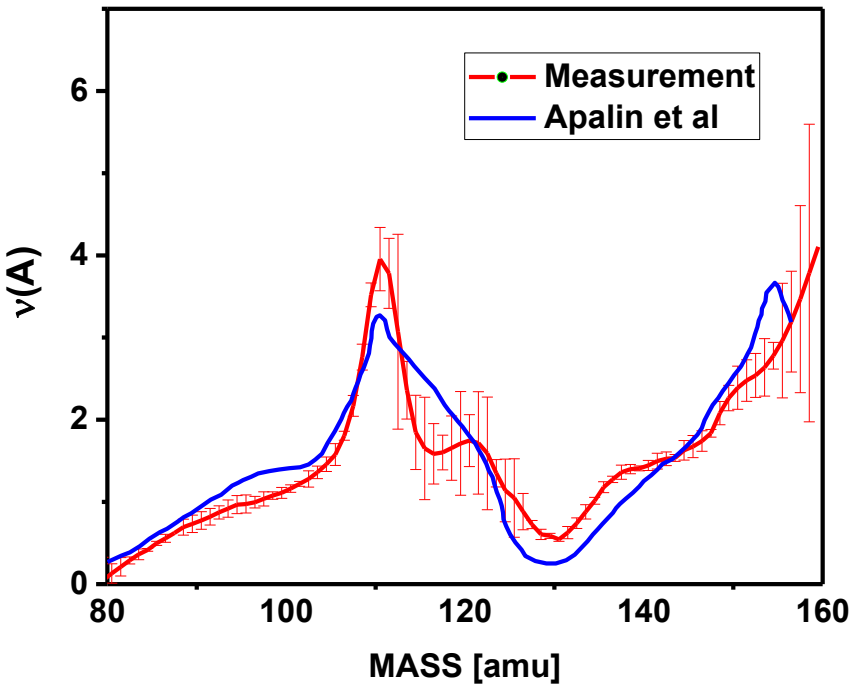

FF mass and Energy values were corrected in iterative procedure for recoil according to
A. Gavron, Nucl. Instrum. and Meth., 115 (1974) 99

14. PFN multiplicity on FF TKE evaluation from measured data

$$\bar{\nu}(TKE) = \int_0^{\infty} \frac{Yc(A,TKE,V_{LAB}) \bullet V_{CM} \bullet (V_{LAB} - V_F \bullet \cos(\Theta))}{\varepsilon(V_{LAB}) \bullet V_{LAB}^2} dV_{LAB} dA \Big/ \int_0^{\infty} Y(A,TKE) dA$$

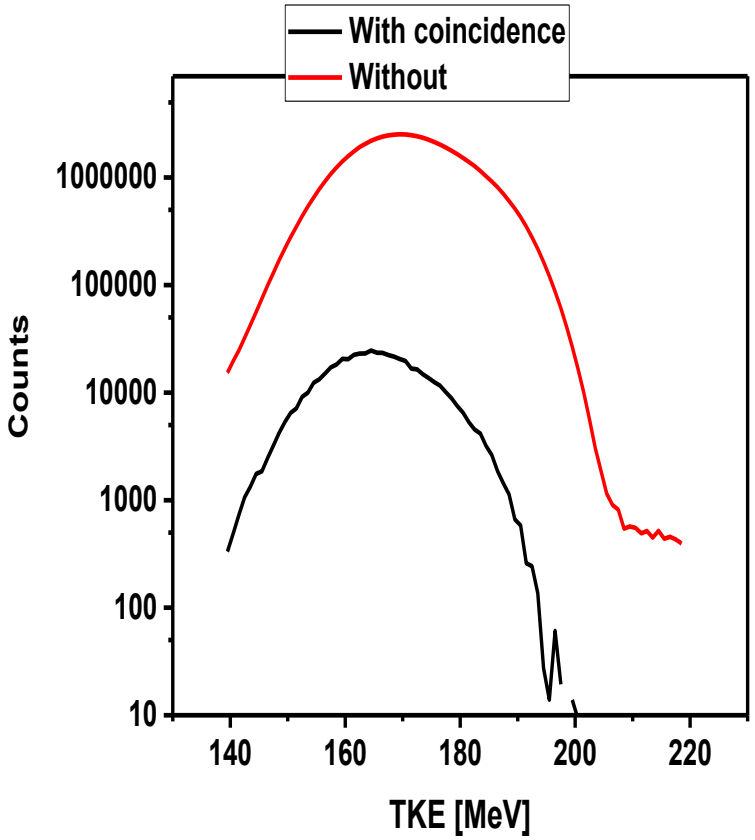

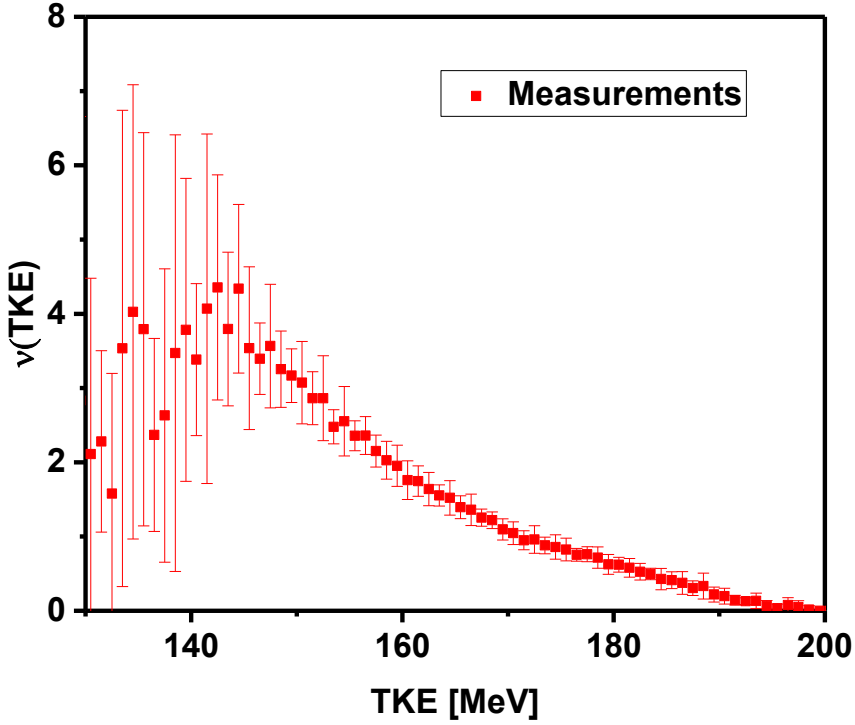

15. Pulse shape separation of PFN from PFG in 252CF(sf) experiment

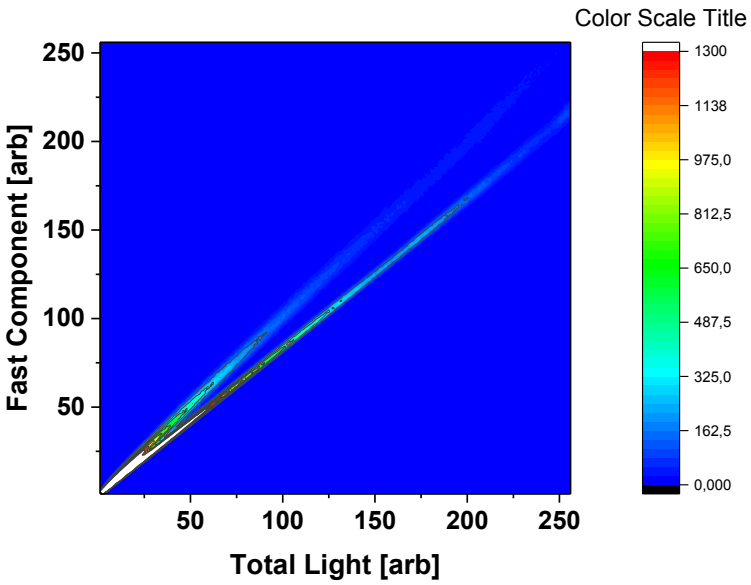

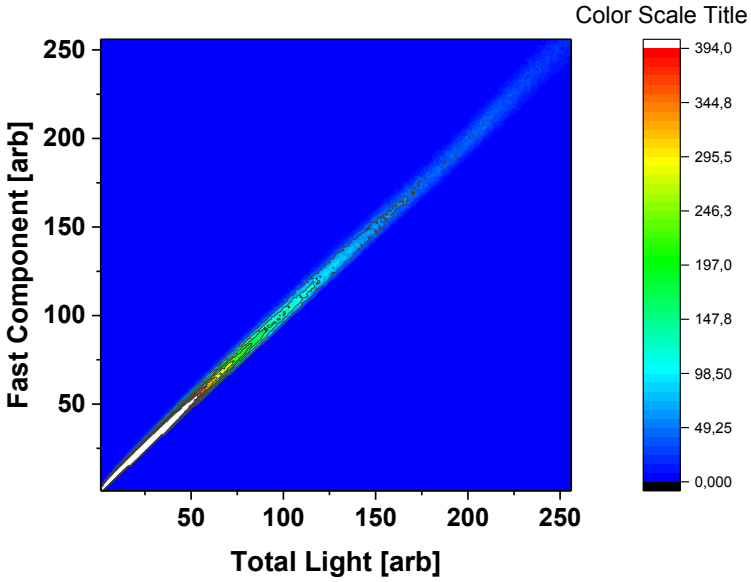

The two window algorithm (fast and total light output component) was implemented and resulted function *ND(Fast,Total)* was plotted on the left figure. demonstrates the function *ND(Fast,Total) i*n rotated according to equation

16. TOF distribution evaluation after pulse shape analysis

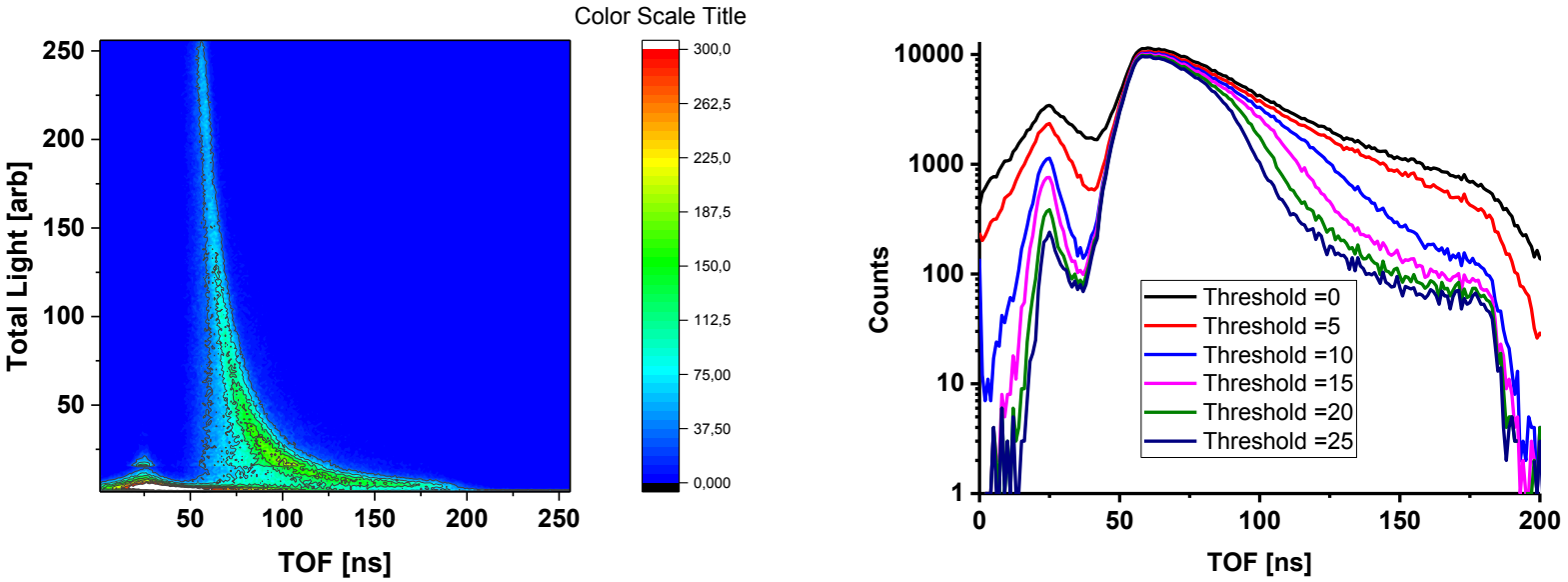

The left figure demonstrates two dimensional distribution of ND pulses in coordinates TOF, Total Light after the pulse shape algorithm was implemented. The right figure demonstrates the TOF distribution obtained after integrating the 2D distribution over Total Light applying thresholds as indicated on the figure. It should be noticed that increase of the threshold reduces the background in high energy part of the TOF. Simultaneously the rise in the threshold for low energy part was observed. Interestingly to see the limit, which reached approximately at the same level both for high and low energy parts of this distribution. This limit was found to be belonging to so cold non-correlated background originated from undetected by ionization chamber FF.

17. Evaluation of neutron detection efficiency for 252CF(sf)

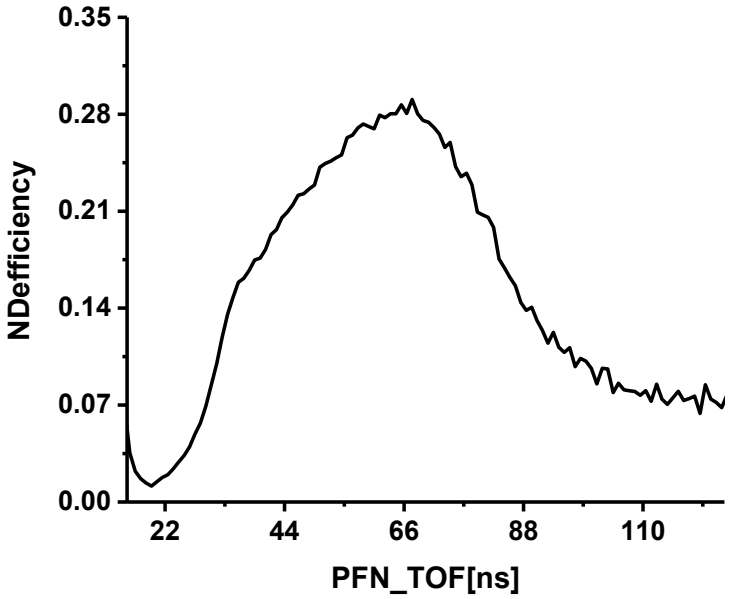

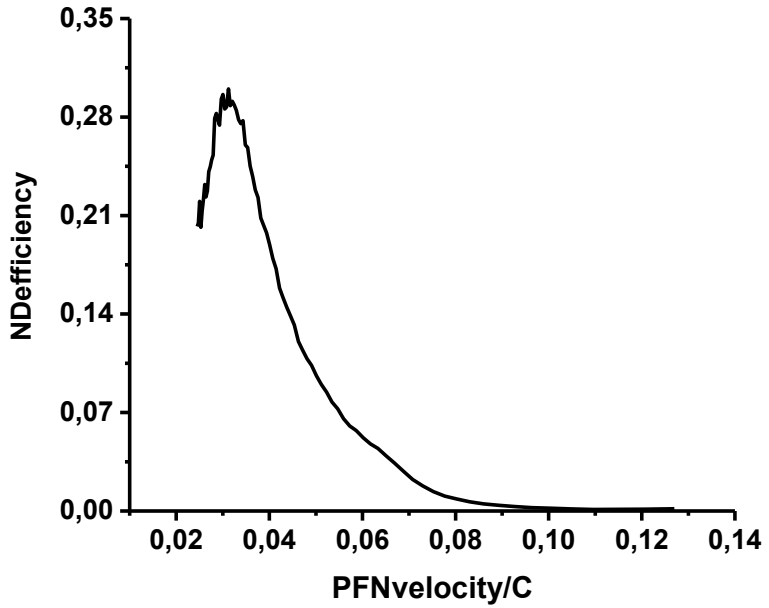

Such a background was first was studied and explained in publication of PTB team in NIM A274 (1989) 217-221. This paper explain how the background can be evaluated and subtracted from the measured data. In our experiments we subtracted the background before correcting the neutron detector efficiency dependence on FF velocity.

18. PFN multiplicity on FF mass and TKE evaluation from measured data

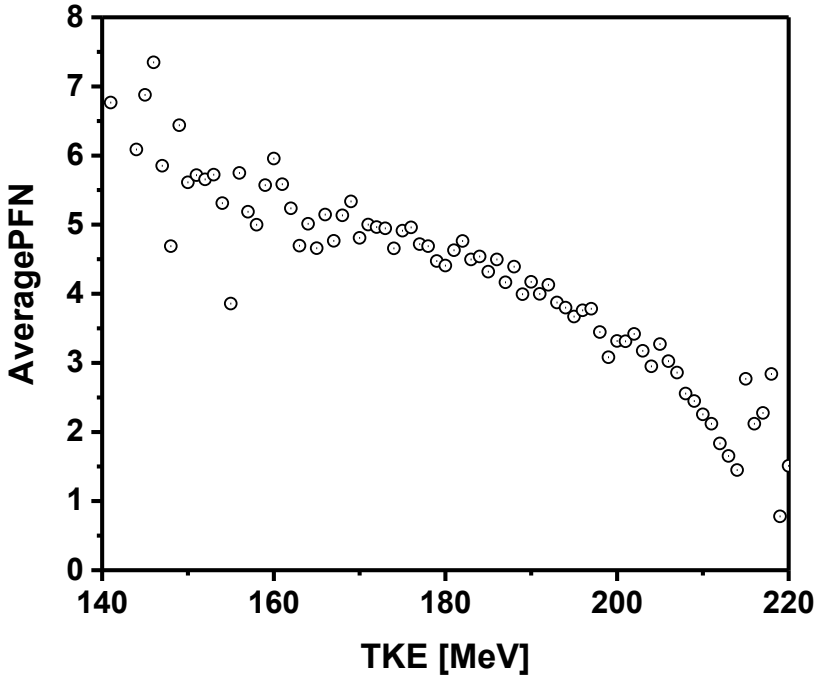

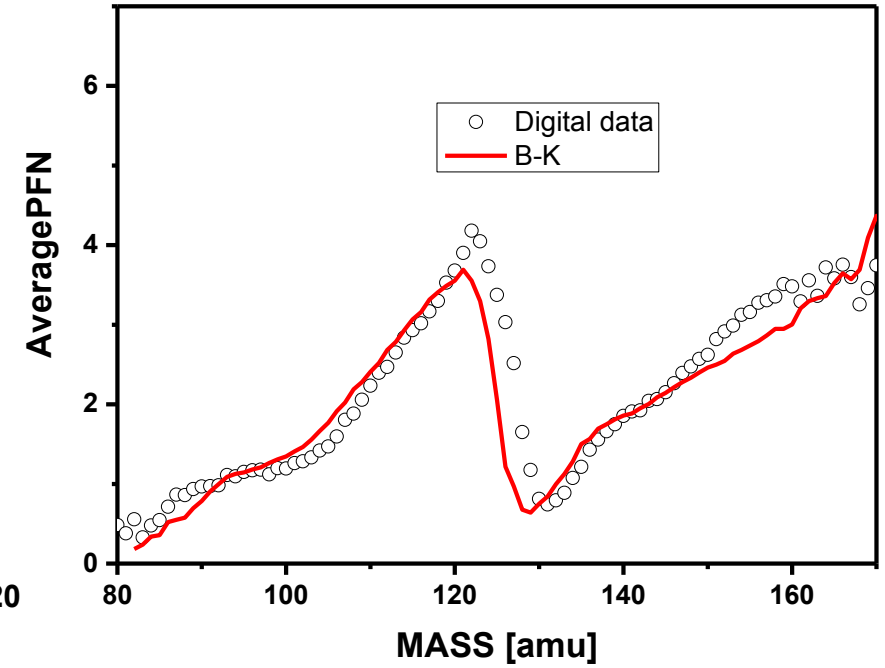

19. Conclusions

The digital data acquisition system was developed and tested in quite difficult experiment.

The digital pulse processing algorithms was developed and tested both on-line and off-line.

The software for PFN multiplicity analysis was revised and some found bugs were removed

The result obtained in this work are differ from the literature and it forces us to revise all stage of new development to verify or improve our recent result.

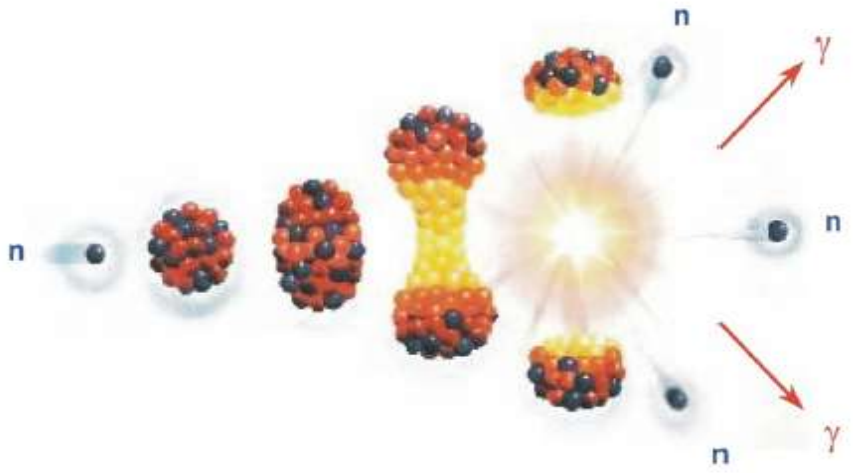

Thank you for your attention ☺